

Covalent Organic Frameworks

Ultrafast and Stable Proton Conduction in Polybenzimidazole Covalent Organic Frameworks via Confinement and Activation

Juan Li, Jing Wang, Zhenzhen Wu, Shanshan Tao, and Donglin Jiang*

Abstract: Polybenzimidazoles are engineering plastics with superb thermal stability and this specificity has sparked a wide-ranging research to explore proton-conducting materials. Nevertheless, such materials encounter challenging issues owing to phosphoric acid proton carrier leakage and slow proton transport. We report a strategy for designing porous polybenzimidazole frameworks to address these key fundamental issues. The built-in channels are designed to be one-dimensionally extended, unidirectionally aligned, and fully occupied by neat phosphoric acid, while the benzimidazole walls trigger multipoint, multichain, and multitype interactions to spatially confine a phosphoric acid network in pores and facilitate proton conduction via deprotonation. The materials exhibit ultrafast and stable proton conduction for low proton carrier content and activation energy—a set of features highly desired for proton transport. Our results offer a design strategy for the fabrication of porous polybenzimidazoles for use in energy conversion applications.

Introduction

Proton-conducting materials are key to fuel cells that transform chemical energy to electricity in a direct, green, and efficient way. Anhydrous proton-conducting materials work at temperatures above 100 °C, enable fast kinetics, and improve efficiency.^[1,2] Researchers have been focused on thermally robust engineering plastics in developing anhydrous proton-conducting materials. Polybenzimidazoles have been the focus of typical engineering plastics for constructing anhydrous proton-conducting systems in conjunction with neat phosphoric acid (H₃PO₄) as proton carrier over the past six decades.^[2,3] However, polybenzimidazoles hardly organize to form a structure which can stabilize the H₃PO₄ network and are facing structure-related bottlenecks. For example, the leakage of H₃PO₄ is a result of polymer chain swollen while

slow proton motion is related to the steric hindrance of swollen polymer chains. As a result, the materials are unstable in performance and reach a proton conductivity of 10⁻² S cm⁻¹, which is even one order of magnitude lower than neat H₃PO₄ (≈ 10⁻¹ S cm⁻¹).^[1-3] These fatal issues greatly deteriorate their practical implementations.^[3] Proton conduction below 100 °C under different relative humidity has been well established with Nafion.^[4] Compared to proton conduction in the presence of water, anhydrous proton transport is far more difficult to establish as it imposes severe conditions on the stability of materials.^[1,2]

Covalent organic frameworks (COFs) are a class of crystalline porous polymer which can develop well-defined skeletons and ordered pores.^[5,6] The porous structures with controlled pore size, shape, environment, and interface render the COF materials able to load a diversity of different proton carriers, such as inorganic acids and imidazole-based organic heterocycles, for the construction of proton-conducting systems.^[6,7] However, most examples have been developed for proton conduction under different humidity.^[6,7c,d] The presence of water facilitates proton conduction, which however, limits the upper working temperature up to 100 °C. Anhydrous proton conduction enables to operate at temperatures above 100 °C but examples are limited to only a few COFs.^[7] Designing COFs to merge stability and anhydrous proton conductivity into one material remains a challenge.

Here we report a strategy for designing porous polybenzimidazole COFs to enable stable yet ultrafast anhydrous proton conduction, which addresses the problems and breaks the upper proton conductivity limit of traditional polybenzimidazole systems. The frameworks are designed to build specific channel walls which can trigger multipoint, multichain, and multitype interactions to lock and stabilize the H₃PO₄ network in pores via spatial confinement and facilitate proton transport via protonation–deprotonation activation. We found that the polybenzimidazole COFs in conjunction with neat H₃PO₄ exhibit stable and ultrafast proton conduction over a wide range of temperatures above 100 °C at a low activation energy and a low H₃PO₄ content. These features are highly desired to be combined in proton-conducting materials and demonstrate a new platform for designing porous polybenzimidazole materials for advanced energy conversions.

Results and Discussion

Design Strategy. We integrated benzimidazole units into the backbone to construct stable COFs with one-dimensional (1D) and unidirectionally aligned channels which are fully

[*] Dr. J. Li, J. Wang, Z. Wu
Institute of Crystalline Materials, Shanxi University
Wucheng Rd No 92, Taiyuan 030006 (China)

Dr. S. Tao, Prof. D. Jiang
Department of Chemistry, Faculty of Science
National University of Singapore
3 Science Drive 3, Singapore 117543 (Singapore)
E-mail: chmjd@nus.edu.sg

Prof. D. Jiang
Joint School of National University of Singapore and Tianjin
University, International Campus of Tianjin University
Binhai New City, Fuzhou 350207 (China)

 Supporting information and the ORCID identification number(s) for the author(s) of this article can be found under:
 <https://doi.org/10.1002/anie.202101400>.

accessible to neat H_3PO_4 (Figure 1 a). One distinct feature is that the pore walls are designed to possess imine linkages and benzimidazole units which stack along the z direction, so that each channel consists of six single file N chains, three N-H chains, and three imidazolium cation chains. The imine linkage owing to the presence of nitrogen atom serves as hydrogen-bonding acceptor to develop single point hydrogen-bonding interactions with H_3PO_4 .^[7c] In contrast, the benzimidazole chains trigger multipoint, multichain, and multitype electrostatic and hydrogen-bonding interactions with the H_3PO_4 network (Figure 1 b)^[2d,8] to stabilize and lock the H_3PO_4 networks in the pores, as evidenced by single crystal structure of benzimidazole– H_3PO_4 complex (Figure 1 c). Such a high level of multiple hierarchical interactions has not been realized with other COFs so far reported. More importantly, the N atom in the benzimidazole unit is protonated to form imidazolium cation while H_3PO_4 is deprotonated to form H_2PO_4^- anion (Figure 1 c), so that the proton network is activated by the H^+ and open H_2PO_4^- sites to facilitate proton conduction. We highlight that this wall configuration offers the structure basis for stabilizing proton networks in the pores and for constituting proton-conducting freeways to enable ultrafast proton transport. Clearly, this strategy merges the advantages of both COFs and polybenzimidazoles into one material and enables to address the key fundamental issues of

conventional polybenzimidazoles. As a result, we observed that the COF systems exhibit ultrafast anhydrous proton conduction over a wide range of temperatures above 100 °C.

Synthesis. We synthesized polybenzimidazole TPB-DABI-COF (Figure 1 a) by condensing 1,3,5-tris(4-formylphenyl)benzene (TPB) knot with 2,5-diamino-3,4-dimethylbenzimidazole (DABI) linker under solvothermal conditions. In detail, polycondensation of TPB with DABI in a mixture of *o*-dichlorobenzene/*n*-butanol (1/1 vol.) in the presence of acetic acid (6 M) at 120 °C for 3 days produced TPB-DABI-COF as dark yellow solid with 75 % isolation yield (Supporting Information).

Fourier-transform infrared spectroscopy (FTIR) of TPB-DABI-COF revealed that the N-H stretching bands at 3323 and 3401 cm^{-1} of DABI (Figure 2 a, blue curve) and the C=O vibration band at 1694 cm^{-1} of TPB (Figure 2 a, black curve) disappeared, suggesting the occurrence of polycondensation reaction. The new vibration bands at 1621 cm^{-1} was assigned to the C=N bond (Figure 2 a, red curve), indicating the formation of imine linkage. Solid-state ^{13}C cross polarization magic angle spinning nuclear magnetic resonance (CP/MAS NMR) spectroscopy of TPB-DABI-COF revealed a signal at 12.71 ppm which was assigned to the methyl carbon of the benzimidazole linker, together with a peak at 141.01 ppm which was attributed to the carbon atom of the C=N linkage

(Figure 2 b). The high-resolution transmission electron microscopy (HRTEM) showed a clear diffraction pattern (inset) and ordered channels of 2.5 nm (Figure 2 c). Thermogravimetric analysis demonstrated that it is thermally robust and does not decompose up to 400 °C under nitrogen (Supporting Information, Figure S1), which is comparable to those of polybenzimidazoles.^[2]

Crystalline Structure. The crystalline structure and unit cell parameters of TPB-DABI-COF were determined by powder X-ray diffraction measurements (PXRD) in conjunction with structural simulations using density functional theory tight binding (DFTB+) and Pawley refinements. TPB-DABI-COF exhibited a PXRD pattern with intense peaks at 2.92°, 5.02°, 5.75°, 7.57°, 9.91°, and 24.1°, which were assigned to the (100), (110), (200), (210), (220), and (001) facets, respectively (Figure 3 a, black curve). DFTB+ calculations revealed that TPB-DABI-COF adopts a space group of P_3 with unit-cell parameters of $a=b=39.4722 \text{ \AA}$, $c=4.0861 \text{ \AA}$, $\alpha=\beta=90^\circ$, and $\gamma=120^\circ$. The atomistic coordinates of AA-stacking TPB-

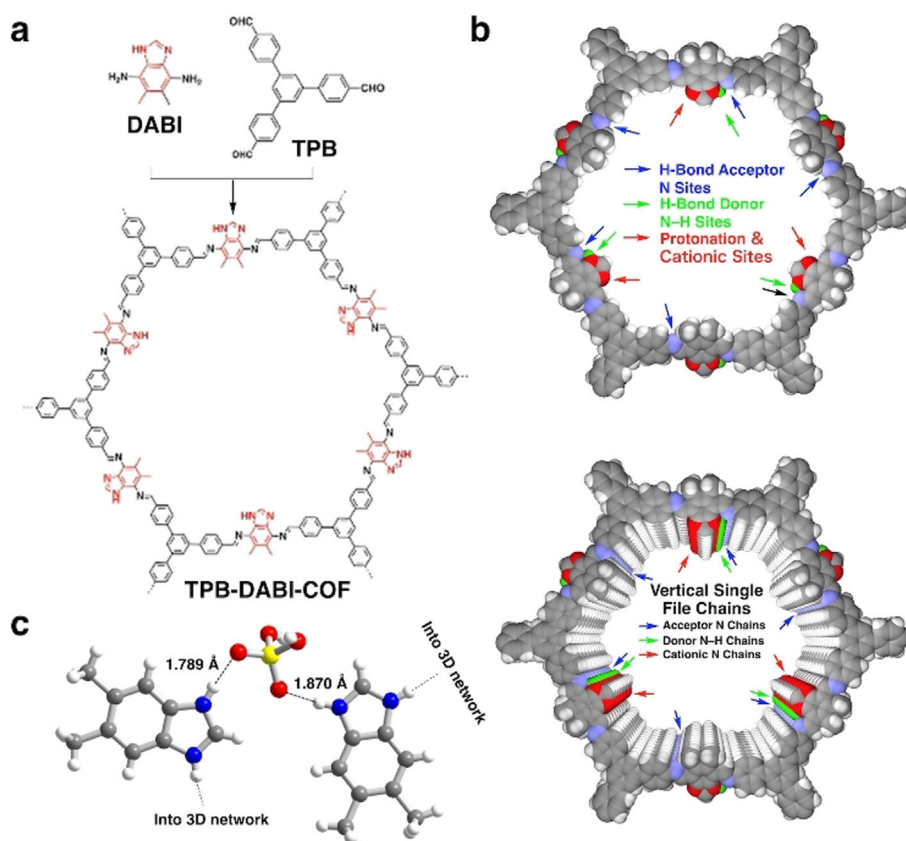


Figure 1. a) Depiction of the polybenzimidazole COF (TPB-DABI-COF). b) Reconstructed structures of a single layer (top panel) and ten layers (bottom panel) of the TPB-DABI-COF and sites and vertical single file chains to confine and activate the H_3PO_4 network. c) Single-crystal structure of the benzimidazole– H_3PO_4 complex shows N–H...O hydrogen-bond and electrostatic interactions; one N of the imidazole ring is protonated by H_3PO_4 . Atom key: N (blue), O (red), H (white).



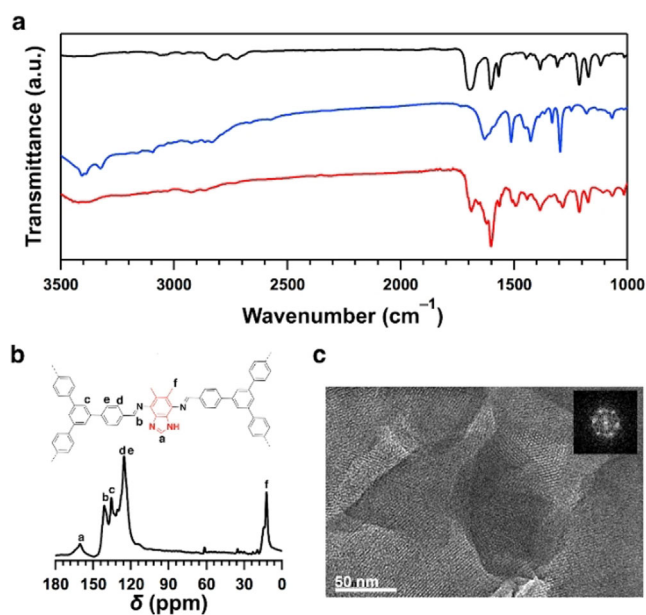


Figure 2. a) FTIR spectra of TPB (black), DABI (blue), and TPB-DABI-COF (red). b) Solid-state ¹³C CP/MAS NMR spectrum of TPB-DABI-COF and peak assignment. c) HRTEM image of TPB-DABI-COF. Inset: the fast Fourier transform (FFT) spectrum.

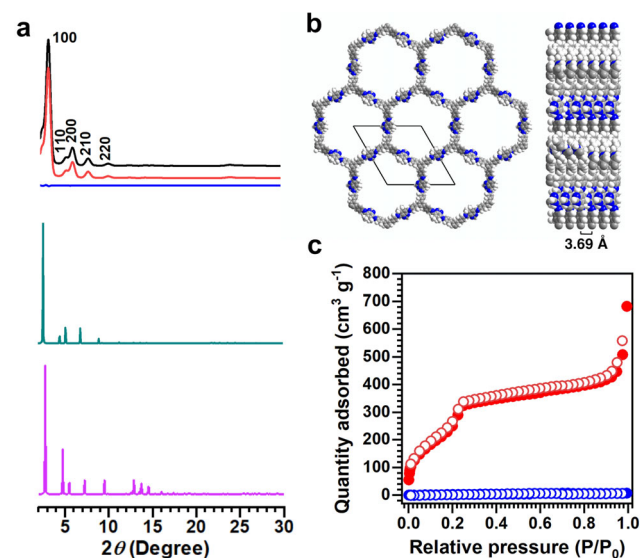


Figure 3. a) PXRD patterns of TPB-DABI-COF of the experimentally observed (black), Pawley refined (red) and their difference (blue), simulated using the AA (green), and staggered AB (purple) stacking modes. b) Top and side views of reconstructed structure of TPB-DABI-COF with seven pores and six layers. Atom key: N (blue), C (gray), H (white). c) N₂ adsorption isotherm curves of TPB-DABI-COF (red circles; filled: adsorption, open: desorption) and H₃PO₄@TPB-DABI-COF (blue circles; filled: adsorption, open: desorption).

DABI-COF are summarized in the Supporting Information, Table S1. The AA-stacking mode yields a PXRD pattern (Figure 3a, green curve) which agrees well with the observed profile. In contrast, the AB-stacking mode (Figure 3a, purple curve) cannot reproduce the PXRD data.

Pawley refinements yielded a PXRD pattern (Figure 3a, red curve) that is consistent with the experimentally observed PXRD profile to show only a small difference (Figure 3a, blue curve) with the R_{WP} and R_p values of 0.58% and 0.42%, respectively. The presence of the (001) facet at 24.1° reveals the structural ordering with an interval of 3.689 Å along the z direction perpendicular to the 2D polymer plane. The reconstructed crystal structure reveals mesoporous channels that are extended and aligned across the material while the pore walls are installed with dense benzimidazole blocks (Figure 3b,c). This channel configuration paves the chemical basis for triggering multipoint, multichain, and multitype hydrogen bonding and electrostatic interactions with the H₃PO₄ network in each channel (Figure 1b). Such a network has not been explored by COFs.^[7]

Nitrogen sorption isotherm curves (Figure 3c, red circles) revealed that TPB-DABI-COF possesses a Brunauer–Emmett–Teller (BET) surface area of 865.2 m² g⁻¹, a pore size of 2.4 nm, and a pore volume of 1.06 cm³ g⁻¹ (Figure S2, Table S2).

Chemical Stabilities. We examined the chemical stability by immersing the TPB-DABI-COF samples in THF, boiling water, and aqueous HCl solution (9 M), respectively. After seven days, we measured PXRD and observed that TPB-DABI-COF retains its crystallinity as evidenced by unchanged peak positions and full width at half maximum (Figure S3). Nitrogen sorption measurements revealed that the porosity of the COF samples is retained under these conditions (Figure S4). We further investigated the stability of TPB-DABI-COF in neat H₃PO₄ by loading H₃PO₄ into the pores at 120 °C for seven days. Surprisingly, TPB-DABI-COF kept its crystallinity (Figures S3) and porosity (Figure S4). These results indicate that TPB-DABI-COF is stable to retain structure and is robust to explore anhydrous proton conduction. We further examined the anti-oxidation capability of TPB-DABI-COF by Fenton test and confirmed that TPB-DABI-COF hardly changes its crystallinity and porosity (Figures S3 and S5).

Single Crystal Structure. In order to identify the interactions between H₃PO₄ and benzimidazole unit, we succeeded in preparing single crystals of the model complex of benzimidazole and H₃PO₄ (Figure 1c; Supporting Information). From the single crystallography (Table S3, CCDC 194985^[9]), we observed that one nitrogen atom of benzimidazole is protonated to form imidazolium cation while H₃PO₄ is deprotonated into H₂PO₄⁻ anion; these two ionic species are interacted via electrostatic interaction in the complex. This protonation–deprotonation process yields H₂PO₄⁻ open sites for facilitated proton transport. Moreover, these two species further form two hydrogen-bonding interactions between the N–H units of benzimidazole ring and the P=O bonds of H₂PO₄⁻ anion (Figure 1c).

Loading H₃PO₄ into COFs and Characterizations. As the pore volume reflects the space that is accessible to H₃PO₄, we used the pore volume of TPB-DABI-COF to determine the maximum loading content of H₃PO₄ in the pores. From the density of neat H₃PO₄ (1.834 g cm⁻³) and the pore volume (1.06 cm³ g⁻¹) of TPB-DABI-COF, the maximum H₃PO₄ loading content is 66.1 wt%. Experimentally, we used neat

H_3PO_4 crystals and a vacuum impregnation method (Supporting Information) to load into the channels of TPB-DABI-COF and prepared H_3PO_4 @TPB-DABI-COF.^[7e] The resulting H_3PO_4 @TPB-DABI-COF samples exhibited a negligible porosity (Figure 3c, blue circles; Table S2), indicating that the pores of TPB-DABI-COF are fully filled with H_3PO_4 . FTIR spectroscopy confirmed the presence of H_3PO_4 as evidenced by new stretching and in-plane bending vibration bands of the P=O bond of H_2PO_4^- anion at 980 and 498 cm^{-1} , respectively (Figure S7). Noticeably, the vibration band of the C=N bond shifted to 1649 cm^{-1} (Figure S7), suggesting that the N atom of the C=N linkage forms hydrogen-bonding interaction with H_3PO_4 .^[7e]

We further disclosed the interactions between H_3PO_4 and TPB-DABI-COF by using X-ray photoelectron spectroscopy (XPS). The high-resolution N 1s spectra of TPB-DABI-COF (Figure 4a) revealed two peaks at 399.45 and 400.35 eV, which were assigned to the N atoms of the imine C=N bond and of benzimidazole -C=N- bond, respectively.^[10] The high-resolution N 1s spectra of H_3PO_4 @TPB-DABI-COF showed that the benzimidazole -C=N- bond is shifted from 400.35 to 401.03 eV, reflecting the ionization of benzimidazole into imidazolium cation, while the imine C=N bond is also shifted to 401.03 eV, suggesting the hydrogen bonding interactions with H_3PO_4 (Figure 4b). The binding energies for C 1s spectra of TPB-DABI-COF and H_3PO_4 @TPB-DABI-COF are observed at 284.9, 286.1, and 286.6 eV (Figure 4c,d). The first and second peaks are attributed to the C=C and C=N bonds in the COF skeleton. The peak at 286.6 eV (Figure 4d) was assigned to the carbon atom bonded to charged nitrogen atoms (C=NH⁺).^[11] The P 2p XPS spectrum of H_3PO_4 @TPB-DABI-COF was deconvoluted into two peaks at 134.2 and 135.0 eV, which were assigned to the phosphorus atoms of H_2PO_4^- and H_3PO_4 , respectively (Figure S8).^[12,13] Together with the single crystal structure, these analyses unambiguously revealed multiple hierarchical interactions between polybenzimidazole walls with the H_3PO_4 networks.

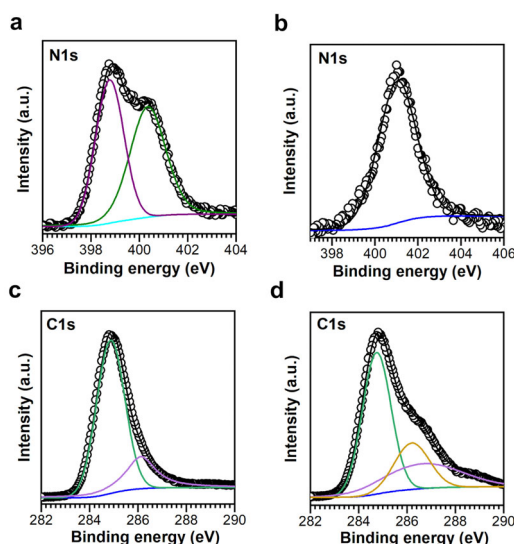


Figure 4. High-resolution XPS spectra of the a) N 1s band of TPB-DABI-COF, b) N 1s band of H_3PO_4 @TPB-DABI-COF, c) C 1s band of TPB-DABI-CO, and d) C 1s band of H_3PO_4 @TPB-DABI-COF.

High-angle annular dark-field scanning TEM images confirmed a homogeneous distribution of C, N, O, and P elements in H_3PO_4 @TPB-DABI-COF (Figure S9). Thus, H_3PO_4 @TPB-DABI-COF enables spatial confinement and activation of the H_3PO_4 network by the imine-linked polybenzimidazole walls.

Impedance Studies and Anhydrous Proton Conduction.

We utilized impedance measurements to investigate the conductivity of the pristine TPB-DABI-COF without installation of H_3PO_4 by pressing the TPB-DABI-COF sample into a round pellet under nitrogen. We observed that TPB-DABI-COF itself is an insulator to show a resistance of 30 M Ω which precludes any proton and/or electric conductivity (Figure S6). Thus, TPB-DABI-COF is suitable as a proton-conducting material.

We prepared pellets of H_3PO_4 @TPB-DABI-COF by pressing the H_3PO_4 @TPB-DABI-COF samples under 200 kN for 30 min under nitrogen and measured proton conductivity by alternating-current impedance spectroscopy under anhydrous condition under nitrogen. The Nyquist plots of H_3PO_4 @TPB-DABI-COF under anhydrous condition were recorded by varying temperature from 100 to 160 °C. The intercepts on the Z' axis was identified as the resistance. The proton conductivity was calculated using the equation $\sigma = L/SR$, where σ is the proton conductivity, L is the pellet thickness (cm), S is the electrode area (cm^2), and R is the resistance (Ω). The proton conductivities were calculated to be 7.37×10^{-2} , 8.59×10^{-2} , 9.71×10^{-2} , 1.09×10^{-1} , 1.22×10^{-1} , 1.39×10^{-1} , and $1.52 \times 10^{-1} \text{ Scm}^{-1}$ at 100, 110, 120, 130, 140, 150, and 160 °C, respectively (Figure 5a; Figure S10, Table S5). Notably, these proton conductivities are even at the same level of neat molten H_3PO_4 ($\approx 10^{-1} \text{ Scm}^{-1}$).^[12]

Polybenzimidazole systems have a proton conductivity that is one order of magnitude lower than that of neat H_3PO_4 , as the swollen polymer chains exert steric hindrance to impede proton motion, while the swollen chains leak H_3PO_4 and result in a low performance stability.^[2d,14,15] These bottlenecks are associated with the structural features of polybenzimidazoles. In contrast, the proton conductivity of H_3PO_4 @TPB-DABI-COF is improved by 1–4 orders of magnitude compared to other systems (Table S4). Among metal-organic frameworks, the highest proton conductivity is $3.0 \times 10^{-3} \text{ Scm}^{-1}$ at 150 °C observed for H_3PO_4 @MIL-101.^[16] The highest anhydrous proton conductivity of H_3PO_4 @COFs is H_3PO_4 @TPB-DMeTP-COF ($1.91 \times 10^{-1} \text{ Scm}^{-1}$ at 160 °C),^[7e] followed by H_3PO_4 @TPB-Azo-COF ($6.70 \times 10^{-5} \text{ Scm}^{-1}$ at 67 °C; Tables S4 and S5).^[6b]

The H_3PO_4 @TPB-DMeTP-COF achieves an anhydrous proton conductivity of $1.91 \times 10^{-1} \text{ Scm}^{-1}$ at 160 °C. The exceptional proton conductivity of H_3PO_4 @TPB-DABI-COF is encouraging as H_3PO_4 @TPB-DABI-COF has a far much low H_3PO_4 content of 66.1 wt %, which is one fourth that of H_3PO_4 @TPB-DMeTP-COF with a H_3PO_4 content of 266.6 wt %. We tested the long-term stability of H_3PO_4 @TPB-DABI-COF at 160 °C for 120 h and observed that the proton conductivity retains the same value as its initial one (Figure 5a, black curve; Figure S11). We plotted the proton conductivity versus temperature to examine the temperature dependency. As shown in Figure 5d (black curve), an



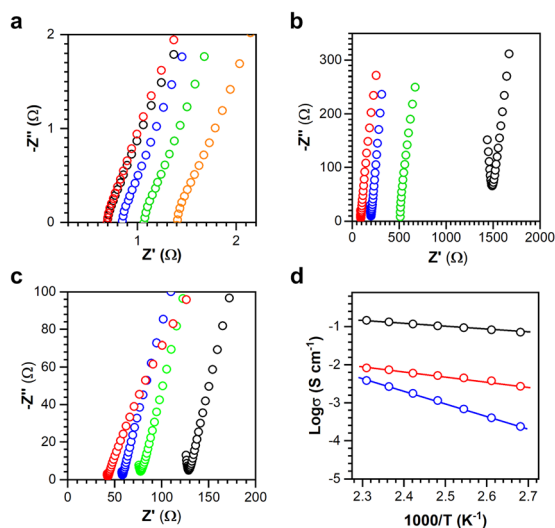


Figure 5. a) Nyquist plots of H_3PO_4 @TPB-DABI-COF at 100 °C (orange), 120 °C (green), 140 °C (blue), 160 °C (red) and 160 °C after a 120 h run (black). b) Nyquist plots of H_3PO_4 @TPB-DABI-POP at 100 °C (orange), 120 °C (green), 140 °C (blue), and 160 °C (red). c) Nyquist plots of 42.9 wt% H_3PO_4 @TPB-DABI-COF at 100 °C (orange), 120 °C (green), 140 °C (blue), and 160 °C (red). d) Arrhenius plots of H_3PO_4 @TPB-DABI-COF (black), 42.9 wt% H_3PO_4 @TPB-DABI-COF (red), and H_3PO_4 @TPB-DABI-POP (blue).

Arrhenius-type linear curve is deduced. From the slope of the curve, the activation energy was evaluated to be 0.17 eV. This result suggests a hopping mechanism for the proton to transport over the H_3PO_4 network in the nanochannels. Notably, this activation energy is lower than that (0.34 eV) of H_3PO_4 @TPB-DMeTP-COF and thus enables high-rate proton conduction over a wide range of temperature over 100 °C. Indeed, H_3PO_4 @TPB-DABI-COF exhibits higher conductivities than H_3PO_4 @TPB-DMeTP-COF from 100 to 130 °C.^[7c] These results suggest that H_3PO_4 @TPB-DABI-COF is unique as it combines ultrafast proton conductivity, high stability, low proton carrier content, and low activation energy—a set of attractive features that are highly desired to be combined in one material.

Comparative and Control Studies. In order to demonstrate the importance of being ordered porous structure, we synthesized an amorphous version TPB-DABI-POP as a control, which is amorphous (Figures S12) and has a different microscopic image from that of crystalline TPB-DABI-COF (Figure S13). TPB-DABI-POP exhibited a BET surface area of $275.01 \text{ m}^2 \text{ g}^{-1}$ and a pore volume of $0.41 \text{ cm}^3 \text{ g}^{-1}$ (Figures S14 and S15, Table S2). By using the same protocol, TPB-DABI-POP was loaded with H_3PO_4 to yield H_3PO_4 @TPB-DABI-POP that contains 42.9 wt% H_3PO_4 . H_3PO_4 @TPB-DABI-POP exhibited proton conductivities of 2.38×10^{-4} , 4.00×10^{-4} , 6.87×10^{-4} , 1.15×10^{-3} , 1.78×10^{-3} , 2.70×10^{-3} , and $3.87 \times 10^{-3} \text{ S cm}^{-1}$ at 100, 110, 120, 130, 140, 150, and 160 °C, respectively (Figure 5b; Figure S16, Table S5).

In order to compare with TPB-DABI-POP system, we prepared 42.9 wt% H_3PO_4 @TPB-DABI-COF with the same

H_3PO_4 content (Table S2). Surprisingly, the proton conductivities of 42.9 wt% H_3PO_4 @TPB-DABI-COF are 2.75×10^{-3} , 3.81×10^{-3} , 4.56×10^{-3} , 5.26×10^{-3} , 6.08×10^{-3} , 7.43×10^{-3} , and $8.35 \times 10^{-3} \text{ S cm}^{-1}$ at 100, 110, 120, 130, 140, 150, and 160 °C, respectively (Figure 5c; Figure S17). Intriguingly, these proton conductivities are two-to-eleven-fold as high as than those of amorphous H_3PO_4 @TPB-DABI-POP under otherwise same conditions.

These results indicate that the COF channels help to form H_3PO_4 networks and promote proton transport. More explicitly, H_3PO_4 @TPB-DABI-POP exhibits an E_a value of 0.61 eV (Figure 5d, blue curve), which is much higher than that (0.23 eV) of 42.9 wt% H_3PO_4 @TPB-DABI-COF (Figure 5d, red curve). The irregular pores of TPB-DABI-POP unlike the 1D channels of TPB-DABI-COF, suppress an efficient extension of hydrogen-bonding H_3PO_4 network. The irregular structure in H_3PO_4 @TPB-DABI-POP leaves sluggish proton motion via a vehicle mechanism.

Conclusion

In summary, we have demonstrated a strategy for designing polybenzimidazole COFs with inherent yet ordered 1D pores to achieve ultrafast yet stable anhydrous proton conduction over a wide range of temperatures above 100 °C. The porous polybenzimidazole frameworks are thermally and chemically stable to enable the spatial confinement of phosphoric acid in the pores. The channel walls trigger multipoint, multichain, and multitype electrostatic and hydrogen-bonding interactions with phosphoric acid networks, so that the proton-conducting systems are not only stabilized but also activated via a protonation–deprotonation process. This configuration not only offers ordered paths to achieve ultrafast proton conduction at a low H_3PO_4 content, but also locks the network to enable stable performance at high temperatures. The polybenzimidazole COFs enable the combination of anhydrous proton conductivity, performance stability, low proton carrier loading content, and low thermal activation energy in one system—a set of attractive features that are highly desired for proton transport. With these distinct features, we envision that COFs offer a way to design well-defined porous polybenzimidazole materials for proton conduction and advanced energy conversion.

Acknowledgements

We gratefully acknowledge financial support from the National Natural Science Foundation of China (21805173, 21975049). D.J. acknowledges a MOE tier 1 grant (R-143-000-A71-114) and NUS startup grant (R-143-000-A28-133).

Conflict of interest

The authors declare no conflict of interest.

Keywords: anhydrous proton conduction · electrostatic interactions · hydrogen-bonding interactions · polybenzimidazoles

- [1] a) K. A. Mauritz, R. B. Moore, *Chem. Rev.* **2004**, *104*, 4535–4586; b) Q. Li, J. O. Jensen, R. F. Savinell, N. J. Bjerrum, *Prog. Polym. Sci.* **2009**, *34*, 449–477; c) D. W. Shin, M. D. Guiver, Y. M. Lee, *Chem. Rev.* **2017**, *117*, 4759–4805.
- [2] a) M. F. H. Schuster, W. H. Meyer, *Annu. Rev. Mater. Res.* **2003**, *33*, 233–261; b) D. Mecerreyes, H. Grande, O. Miguel, E. Ochoteco, R. Marcilla, I. Cantero, *Chem. Mater.* **2004**, *16*, 604–607; c) Y. Chen, M. Thorn, S. Christensen, C. Versek, A. Poe, R. C. Hayward, M. T. Tuominen, S. Thayumanavan, *Nat. Chem.* **2010**, *2*, 503–508; d) L. Vilčiauska, M. E. Tuckerman, G. Bester, S. J. Paddison, K. D. Kreuer, *Nat. Chem.* **2012**, *4*, 461–466.
- [3] a) R. Bouchet, E. Siebert, *Solid State Ionics* **1999**, *118*, 287–299; b) A. Carollo, E. Quartarone, C. Tomasi, P. Mustarelli, F. Belotti, A. Magistris, F. Maestroni, M. Parachini, L. Garlaschelli, P. P. Righetti, *J. Power Sources* **2006**, *160*, 175–180; c) J. Weber, K. D. Kreuer, J. Maier, A. Thomas, *Adv. Mater.* **2008**, *20*, 2595–2598.
- [4] a) K. Schmidt-Rohr, Q. Chen, *Nat. Mater.* **2008**, *7*, 75–83; b) R. Devanathan, *Energy Environ. Sci.* **2008**, *1*, 101–119; c) G. He, Z. Li, J. Zhao, S. Wang, H. Wu, M. D. Guiver, Z. Jiang, *Adv. Mater.* **2015**, *27*, 5280–5295; d) G. L. Jackson, D. V. Perroni, M. K. Mahanthappa, *J. Phys. Chem. B* **2017**, *121*, 9429–9436.
- [5] a) X. Chen, K. Geng, R. Liu, K. T. Tan, Y. Gong, Z. Li, S. Tao, Q. Jiang, D. Jiang, *Angew. Chem. Int. Ed.* **2020**, *59*, 5050–5091; *Angew. Chem.* **2020**, *132*, 5086–5129; b) P. J. Waller, F. Gándara, O. M. Yaghi, *Acc. Chem. Res.* **2015**, *48*, 3053–3063; c) N. Huang, P. Wang, D. Jiang, *Nat. Rev. Mater.* **2016**, *1*, 16068; d) Z. Li, T. He, Y. Gong, D. Jiang, *Acc. Chem. Res.* **2020**, *53*, 1672–1685; e) D. Jiang, *Chem* **2020**, *6*, 2461–2483; f) D. Rodríguez-San-Miguel, C. Montoro, F. Zamora, *Chem. Soc. Rev.* **2020**, *49*, 2291–2302; g) S. Tao, D. Jiang, *CCS Chem.* **2020**, *2*, 2003–2024.
- [6] a) H. Ma, B. Liu, B. Li, L. Zhang, Y.-G. Li, H.-Q. Tan, H.-Y. Zang, G. Zhu, *J. Am. Chem. Soc.* **2016**, *138*, 5897–5903; b) S. Chandra, T. Kundu, S. Kandambeth, R. BabaRao, Y. Marathe, S. M. Kunjir, R. Banerjee, *J. Am. Chem. Soc.* **2014**, *136*, 6570–6573; c) W. Kong, W. Jia, R. Wang, Y. Gong, C. Wang, P. Wu, J. Guo, *Chem. Commun.* **2019**, *55*, 75–78; d) K. C. Ranjeesh, R. Illathvalappil, S. D. Veer, J. Peter, V. C. W. Goudappagouda, K. V. Raj, S. Kurungot, S. S. Babu, *J. Am. Chem. Soc.* **2019**, *141*, 14950–14954; e) Y. Yang, X. He, P. Zhang, Y. H. Andaloussi, H. Zhang, Z. Jiang, Y. Chen, S. Ma, P. Cheng, Z. Zhang, *Angew. Chem. Int. Ed.* **2020**, *59*, 3678–3684; *Angew. Chem.* **2020**, *132*, 3707–3713.
- [7] a) H. Xu, S. Tao, D. Jiang, *Nat. Mater.* **2016**, *15*, 722–726; b) X. Wu, Y.-l. Hong, B. Xu, Y. Nishiyama, W. Jiang, J. Zhu, G. Zhang, S. Kitagawa, S. Horike, *J. Am. Chem. Soc.* **2020**, *142*, 14357–14364; c) S. Chandra, T. Kundu, K. Dey, M. Addicoat, T. Heine, R. Banerjee, *Chem. Mater.* **2016**, *28*, 1489–1494; d) D. B. Shinde, H. B. Aiyappa, M. Bhadra, B. P. Biswal, P. Wadge, S. Kandambeth, B. Garai, T. Kundu, S. Kurungot, R. Banerjee, *J. Mater. Chem. A* **2016**, *4*, 2682–2690; e) S. Tao, L. Zhai, A. D. Wonanke, M. A. Addicoat, Q. Jiang, D. Jiang, *Nat. Commun.* **2020**, *11*, 1981.
- [8] E. Quartarone, P. Mustarelli, *Energy Environ. SPOPCi.* **2012**, *5*, 6436–6444.
- [9] Deposition Number 194985 contains the supplementary crystallographic data for this paper. These data are provided free of charge by the joint Cambridge Crystallographic Data Centre and Fachinformationszentrum Karlsruhe Access Structures service www.ccdc.cam.ac.uk/structures.
- [10] a) I. B. Obot, A. Madhankumar, S. A. Umoren, Z. M. Gasem, *J. Adhes. Sci. Technol.* **2015**, *29*, 2130–2152; b) J. Liu, F. Yang, L. Cao, B. Li, K. Yuan, S. Lei, W. Hu, *Adv. Mater.* **2019**, *31*, 1902264; c) Y. H. Yan, M. B. Chan-Park, Q. Zhou, C. M. Li, C. Y. Yue, *Appl. Phys. Lett.* **2005**, *87*, 213101.
- [11] U. S. Waware, R. Arukula, A. M. S. Hamouda, P. Kasak, *Ionics* **2020**, *26*, 831–838.
- [12] M. Textor, L. Ruiz, R. Hofer, A. Rossi, K. Feldman, G. Hähner, N. D. Spencer, *Langmuir* **2000**, *16*, 3257–3271.
- [13] Y. Aihara, A. Sonai, M. Hattori, K. Hayamizu, *J. Phys. Chem. B* **2006**, *110*, 24999–25006.
- [14] Y. Özdemir, N. Özkan, Y. Devrim, *Electrochim. Acta* **2017**, *245*, 1–13.
- [15] E. Bakangura, L. Wu, L. Ge, Z. Yang, T. Xu, *Prog. Polym. Sci.* **2016**, *57*, 103–152.
- [16] V. G. Ponomareva, K. A. Kovalenko, A. P. Chupakhin, D. N. Dybtsev, E. S. Shutova, V. P. Fedin, *J. Am. Chem. Soc.* **2012**, *134*, 15640–15643.

Manuscript received: January 28, 2021

Revised manuscript received: March 13, 2021

Accepted manuscript online: March 16, 2021

Version of record online: ■ ■ ■ ■ ■ ■ ■ ■ ■ ■

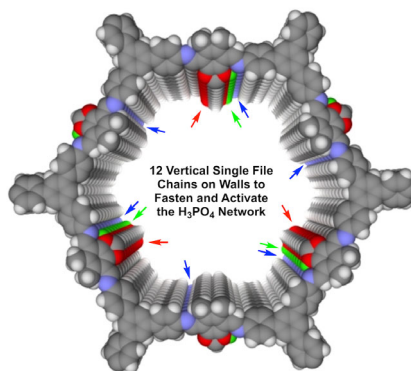
Research Articles



Covalent Organic Frameworks

J. Li, J. Wang, Z. Wu, S. Tao,
D. Jiang* ————— ■■■■-■■■■

Ultrafast and Stable Proton Conduction in
Polybenzimidazole Covalent Organic
Frameworks via Confinement and
Activation



Condensing benzimidazole units via topology-directed polymerization allows the construction of stable covalent organic frameworks with ordered one-dimensional channels. The walls trigger multiple hierarchical interactions so that the proton networks are locked in the pores via spatial confinement and activated via deprotonation. Ultrafast and stable anhydrous proton conduction is achieved over a wide range of temperatures.

